

Stephen F. Austin State University SFA ScholarWorks

Faculty Publications

Biology

2006

The Rotavirus Enterotoxin NSP4 Directly Interacts with the Caveolar Structural Protein Caveolin-1

Rebecca D. Parr

Stephen F Austin State University, parr1@sfasu.edu

Stephen M. Storey

Texas A & M University - College Station

DeAnne M. Mitchell

Texas A & M University - College Station

Avery McIntosh


Texas A & M University - College Station

Minglong Zhou

Texas A & M University - College Station

See next page for additional authors

Follow this and additional works at: <http://scholarworks.sfasu.edu/biology>

 Part of the [Biology Commons](#), and the [Biotechnology Commons](#)

Tell us how this article helped you.

Recommended Citation

Parr, Rebecca D.; Storey, Stephen M.; Mitchell, DeAnne M.; McIntosh, Avery; Zhou, Minglong; Mir, Kiran D.; and Ball, Judith M., "The Rotavirus Enterotoxin NSP4 Directly Interacts with the Caveolar Structural Protein Caveolin-1" (2006). *Faculty Publications*. Paper 48.

<http://scholarworks.sfasu.edu/biology/48>

This Article is brought to you for free and open access by the Biology at SFA ScholarWorks. It has been accepted for inclusion in Faculty Publications by an authorized administrator of SFA ScholarWorks. For more information, please contact cdsscholarworks@sfasu.edu.

Authors

Rebecca D. Parr, Stephen M. Storey, DeAnne M. Mitchell, Avery McIntosh, Minglong Zhou, Kiran D. Mir, and Judith M. Ball

The Rotavirus Enterotoxin NSP4 Directly Interacts with the Caveolar Structural Protein Caveolin-1

Rebecca D. Parr,¹ Stephen M. Storey,¹ DeAnne M. Mitchell,¹ Avery L. McIntosh,²
Minglong Zhou,^{1†} Kiran D. Mir,¹ and Judith M. Ball^{1*}

*Department of Pathobiology¹ and Department of Physiology and Pharmacology,²
Texas A&M University, College Station, Texas*

Received 15 July 2005/Accepted 13 December 2005

Rotavirus nonstructural protein 4 (NSP4) is known to function as an intracellular receptor at the endoplasmic reticulum (ER) critical to viral morphogenesis and is the first characterized viral enterotoxin. Exogenously added NSP4 induces diarrhea in rodent pups and stimulates secretory chloride currents across intestinal segments as measured in Ussing chambers. Circular dichroism studies further reveal that intact NSP4 and the enterotoxic peptide (NSP4₁₁₄₋₁₃₅) that is located within the extended, C-terminal amphipathic helix preferentially interact with caveola-like model membranes. We now show colocalization of NSP4 and caveolin-1 in NSP4-transfected and rotavirus-infected mammalian cells in reticular structures surrounding the nucleus (likely ER), in the cytosol, and at the cell periphery by laser scanning confocal microscopy. A direct interaction between NSP4 residues 112 to 140 and caveolin-1 was determined by the Pro-Quest yeast two-hybrid system with full-length NSP4 and seven overlapping deletion mutants as bait, caveolin-1 as prey, and vice versa. Coimmunoprecipitation of NSP4–caveolin-1 complexes from rotavirus-infected mammalian cells demonstrated that the interaction occurs during viral infection. Finally, binding of caveolin-1 from mammalian cell lysates to Sepharose-bound, NSP4-specific synthetic peptides confirmed the yeast two-hybrid data and further delineated the binding domain to amino acids 114 to 135. We propose that the association of NSP4 and caveolin-1 contributes to NSP4 intracellular trafficking from the ER to the cell surface and speculate that exogenously added NSP4 stimulates signaling molecules located in caveola microdomains.

Rotaviruses (RV) cause severe, life-threatening gastroenteritis in children and animals worldwide and in immunocompromised and elderly adults (46). The RV genome is composed of 11 segments of double-stranded RNA that encodes five nonstructural and six structural proteins (17). Nonstructural protein 4 (NSP4), encoded by RV gene 10, initially was identified as an endoplasmic reticulum (ER) transmembrane glycoprotein essential to RV morphogenesis by serving as an intracellular receptor to double-layered particles (DLPs) (5, 44, 67, 66). NSP4 residues 161 to 175 bind the outer coat protein (VP6) of the DLPs, which facilitates translocation into the ER and the addition of two viral proteins, VP7 and VP4, and a transient ER membrane (40, 66, 67); NSP4 is sufficient for the budding of DLPs into the ER lumen (33). The ER transient viral envelope is eventually removed by an unknown mechanism prior to virus release (40, 44). Because the NSP4 sequence lacks classical ER retention signals and does not appear to be retrieved by retrograde transport and the two N-linked, high-mannose glycosylation sites remain sensitive to endoglycosidase H (endo H) digestion, the current tenet is that NSP4 does not enter or traffic through the Golgi (5, 16).

In addition to facilitating RV maturation at the ER, NSP4 functions as the first described viral enterotoxin that induces diarrhea in neonatal mice and rats in the absence of histolog-

ical alterations (3, 4). The enterotoxic region of NSP4 maps to amino acids (aa) 114 to 135, as determined by functional studies of overlapping synthetic peptides (4). Exogenous addition of intact NSP4 or the enterotoxic peptide NSP4₁₁₄₋₁₃₅ to cultured cells or mouse pup intestinal mucosa triggers a phosphoinositide (PI) signal transduction pathway at the plasma membrane (PM), resulting in the elevation of inositol trisphosphate, intracellular calcium ([Ca²⁺]_i) mobilization, and chloride secretion with fluid loss (11, 15, 41). Endogenous expression of NSP4 or NSP4 fusion proteins likewise elevates [Ca²⁺]_i levels, but by a distinct, phospholipase C-independent mechanism (6, 69).

The functions attributed to NSP4 expression continue to expand. NSP4 and NSP4₁₁₄₋₁₃₅ also affect the sodium-coupled transport of D-glucose and L-leucine, as demonstrated with intestinal brush border membrane vesicles from young rabbits (24). These data suggest that NSP4 interacts with membrane vesicles or vesicle-bound proteins to affect RV pathogenesis. Other data show that NSP4 associates with Triton X-100 detergent-resistant membranes during RV infection, indicating that rafts or caveolae may be involved in NSP4 activity (52). NSP4 has been reported to bind microtubules, block ER-to-Golgi trafficking, and accumulate in microtubule-associated membrane compartments (66, 74). The NSP4 microtubule binding domain maps to the C-terminal 54 residues (129 to 175) (74). In addition, several studies report NSP4-specific seroconversion of immunoglobulin A (IgA) and IgG in RV-infected patients, indicating that NSP4 is exposed to immune cells (51, 75, 76).

Hence, there is increasing evidence that NSP4 is not exclusively localized at the ER but traffics from the ER by a pathway

* Corresponding author. Mailing address: Department of Pathobiology, College of Veterinary Medicine and Biomedical Sciences, TAMU 4467, College Station, TX 77843. Phone: (979) 845-7910. Fax: (979) 845-9231. E-mail: jball@cvm.tamu.edu.

† Present address: Lymphoma Foundation Canada, Vancouver Cancer Center, Vancouver, British Columbia, Canada.

that likely bypasses the Golgi (5, 6, 7, 14, 43). Isolation of an NSP4 cleavage fragment (aa 112 to 175) in culture medium of infected cells further supports the release of endogenously expressed NSP4 from the cell (77). The purified NSP4 fragment initiates PI signaling events and fluid loss, presumably by interacting with the host cell or neighboring cell surface receptors (77). NSP4 also has been shown to interact with the extracellular matrix proteins laminin- β 3 and fibronectin at aa 87 to 145 by yeast two-hybrid assays and coimmunoprecipitation (7). The authors suggest that NSP4 is basolaterally secreted into tissues that underlie the enterocytes to interact with the extracellular matrix.

Circular dichroism spectroscopic experiments demonstrate that NSP4 and NSP4₁₁₄₋₁₃₅ preferentially bind to highly curved, anionic, cholesterol-rich model membrane vesicles that mimic PM caveolae in lipid structure and content (25, 26). In vivo, caveolae are a subset of lipid rafts that are highly curved and rich in cholesterol and sphingomyelin and contain the integral membrane protein caveolin-1 (2). Caveolae are found in most cells, including those of the intestine (18), wherein caveolin-1 forms a scaffold to organize signaling molecules at the PM (2, 49, 54, 57, 63). Key molecular components of Ca²⁺ regulation and signaling are localized to caveolae, including Ca²⁺ ATPase, inositol trisphosphate receptors, tyrosine kinases, G proteins, and calmodulin (2, 21, 50, 53, 54). In addition, caveolae compartmentalize as much as 50% of cellular phosphatidylinositol diphosphate (PIP2) (2, 21, 50, 53, 54) and are the site of PIP2 hydrolysis in response to a ligand (50). Given that NSP4 preferentially binds highly curved, anionic, cholesterol-rich model membranes, promotes PIP2 hydrolysis upon exogenous addition, and disrupts calcium homeostasis, it is reasonable to propose that exogenously added NSP4 interacts with molecules localized to caveola PM microdomains.

The interaction of NSP4 and caveolin-1 was examined by four distinct approaches, (i) laser scanning confocal microscopy (LSCM), (ii) in vivo reverse yeast two-hybrid analyses, (iii) coimmunoprecipitation of RV-infected cells, and (iv) in vitro peptide binding assays. This study localized the caveolin-1 binding domain to an NSP4 region that overlaps other functional domains, including the enterotoxic peptide. LSCM studies further revealed that NSP4 and caveolin-1 colocalize in mammalian cells both in the presence and in the absence of other rotavirus proteins.

MATERIALS AND METHODS

Antibodies. NSP4 and caveolin-1 peptide-specific antibodies were generated in mice, rabbits, or rats as previously described and include mouse anti-NSP4₁₂₀₋₁₄₇ and -NSP4₁₅₀₋₁₇₅; rabbit anti-NSP4₂₋₂₂, -NSP4₁₁₃₋₁₄₉, -NSP4₁₂₀₋₁₄₇, -NSP4₁₅₀₋₁₇₅, and -caveolin-1₂₋₃₂; and rat anti-caveolin-1₁₆₁₋₁₇₈ (25, 64). Rabbit anti-caveolin-1 was purchased from Jackson Immunoresearch Labs Inc. (West Grove, CA) or Transduction Labs (San Diego, CA). Preimmune mouse, rat, and rabbit sera were used as negative controls. Bound antibodies were detected by horseradish peroxidase-labeled goat anti-rabbit or -mouse IgG (Kirkegaard & Perry Laboratories, Inc., Gaithersburg, MD; Pierce, Rockford, IL; Rockland, Gilbertsville, PA), fluorescein isothiocyanate (FITC)-conjugated goat anti-rabbit or -mouse IgG (Kirkegaard & Perry Laboratories, Inc.), or Texas Red-conjugated goat anti-rabbit IgG (Transduction Labs).

Mammalian cell lines. MDCK, Caco-2, and BSC-1 cells were obtained from the American Type Culture Collection (Manassas, VA) and maintained in Dulbecco modified Eagle medium (Gibco, Grand Island, NY) supplemented with 10% fetal bovine serum, L-glutamine (2 mM), penicillin-streptomycin (100 μ g/ml), and nonessential amino acids (Sigma, St. Louis, MO). For confocal imaging

analyses, cells were grown on Lab-Tek chambered-cover glass slides (Nalge Nunc International, Naperville, IL) or coverslips to ~70% confluence. Due to the high expression level of caveolin-1 in MDCK cells (this study), MDCK cell lysates were prepared as a source of caveolin-1. Fischer rat thyroid (FRT) cells that lack expression of caveolin-1 (1, 29) were a kind gift of E. Rodriguez-Boulan (Weill Medical College of Cornell University, New York, NY) and were grown in Coons F12 medium (Sigma) with 10% fetal bovine serum to ~90% confluence. FRT cell lysates served as a caveolin-1-negative mammalian cell control. All cells were utilized prior to 100% confluence and differentiation.

Construction of mammalian plasmids. NSP4 cDNA initially was PCR amplified from pcDNA2.1-NSP4 (gift of M. Estes, Baylor College of Medicine, Houston, TX); the forward and reverse primers were 5'-GATATCAAGATGAAAAGCTTACC GACC-3' and 3'-TTCAGTACGACGTTACTAATTCGAA-5', respectively (the underlined portions are a 3' HindIII site and a 5' EcoRI site). The PCR product was inserted directly into the pcDNA3.1 Topo vector of the eukaryotic TOPO TA cloning kit (Invitrogen, Carlsbad, CA) to generate pcDNA3.1-NSP4, transformed and amplified in TOPO10 cells and sequence verified (Gene Technology Lab, Texas A&M University).

Expression of NSP4 in transiently transfected and RV-infected mammalian cells. MDCK, BSC-1, and Caco-2 cultured cells were transfected with pcDNA3.1-NSP4 with Lipofectamine plus reagent (Gibco, BRL) according to the manufacturer's protocol and incubated at 37°C with 5% CO₂ for 36 h. Expression of NSP4 was verified by Western blot analysis and LSCM imaging (see below).

To examine NSP4 expression in the context of a viral infection, MDCK cells were plated at a density of 10⁵ cells/cm² on sterile glass coverslips, incubated at 37°C in 5% CO₂ for 24 h, and then mock infected or infected with RV SA11 at a multiplicity of infection (MOI) of 4 PFU/cell. At 20 h postinfection (hpi), the cells were washed twice with phosphate-buffered saline (PBS), fixed, and permeabilized for 10 min with methanol-acetone (1:1, vol/vol) at -20°C and stained for LSCM imaging (see below).

Western blot assays. Transiently transfected MDCK, Caco-2, and BSC-1 cells or RV-infected MDCK cells were lysed in RIPA buffer (0.5% sodium deoxycholate, 10% NP-40, 150 mM NaCl, 50 mM Tris, pH 8.0, 0.1% sodium dodecyl sulfate [SDS]) containing the following protease inhibitors: 100 μ M 4-(2-aminoethyl)-benzenesulfonyl fluoride HCl (AEBSF), 80 nM aprotinin, 5 μ M bestatin, 1.5 μ M (2S,3S)-3-((S)-1-[N-(4-guanidinobutyl)carbamoyl]-3-methylbutyl)carbamoyl)oxirane-2-carboxylic acid (E-64), 2 μ M leupeptin, 1 μ M pepstatin A, and 100 μ M phenylmethylsulfonyl fluoride (PMSF) (Calbiochem-Novabiochem Corp., San Diego, CA). Proteins were quantified by bicinchoninic acid assay (Pierce). All lysates were separated by 12% SDS-polyacrylamide gel electrophoresis (PAGE), electroblotted onto nitrocellulose membranes, and blotted with NSP4 peptide- or caveolin-1 peptide-specific antibodies. Reactive bands were visualized by the addition of horseradish peroxidase-conjugated IgG and SuperSignal West Pico chemiluminescent substrate (Pierce), followed by exposure to Kodak X-Omat film (47).

LSCM analyses and colocalization. Before examining for colocalization of NSP4 with caveolin-1, it was important to affirm the expression of caveolin-1 in the cultured cells. Intestinal (Caco-2) and kidney (MDCK, BSC-1) epithelial cell lines were sequentially probed with rabbit anti-human caveolin-1 (Transduction Labs) and goat anti-rabbit-IgG-Texas Red, and the specific fluorescence was monitored by LSCM.

Once caveolin-1 expression was established, pcDNA3.1-NSP4-transfected MDCK, BSC-1, and Caco-2 cells were incubated for 48 h, fixed with methanol-acetone (1:1, vol/vol) at -20°C, blocked with 3% BLOTTO (nonfat dry milk in PBS), and incubated with mouse anti-NSP4₁₂₀₋₁₄₇ (1:200) and rabbit anti-caveolin-1 (1:500; Transduction Labs) to detect NSP4 and caveolin-1, respectively. Goat anti-mouse IgG-FITC and goat anti-rabbit IgG-Texas Red were used to detect the primary antibodies. RV- or mock-infected cells grown on glass coverslips were similarly fixed and permeabilized with methanol-acetone (1:1, vol/vol). The fixed cells were briefly air dried, rinsed in PBS, blocked in 3% BLOTTO, and incubated with mouse anti-NSP4₁₅₀₋₁₇₅ (1:600) and rabbit anti-caveolin-1 (1:200). Goat anti-mouse IgG conjugated to Texas Red and goat anti-rabbit IgG conjugated to FITC were then used to visualize the NSP4 and caveolin-1 antibodies, respectively. All antibodies were diluted in 1% BLOTTO, and incubations were followed with a minimum of four washes with 0.5% BLOTTO, 10 min each. The coverslips were rinsed with PBS and affixed to glass slides with fluorescence microscopy mounting medium (Kirkegaard & Perry Laboratories, Inc.). To control for the specificity of the NSP4 antibody staining, mock-transfected and mock-infected cells were stained with both primary and secondary antibodies.

All cells were visualized with an MRC-124MP Bio-Rad LSCM with a Zeiss Axiovert inverted microscope (Carl Zeiss, Inc., Thornwood, NY), a 63 \times oil Apochromat objective, and the 488-nm excitation line of an argon-krypton ion

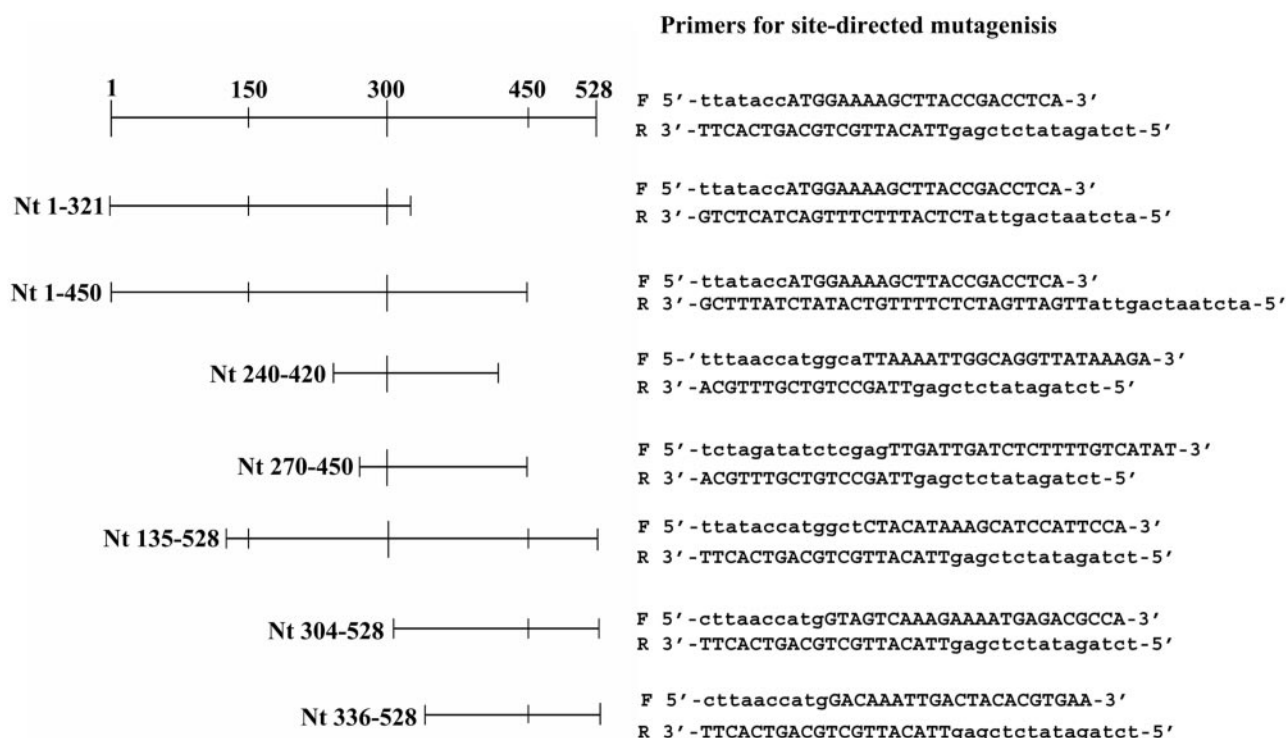


FIG. 1. Linear schematic of RV SA11 full-length NSP4 and deletion mutants with forward and reverse primers. PCR fragments were generated with the forward and reverse primers listed to the right of each construct and were cloned into DBD plasmid pD22 and AD plasmid pD32 of the ProQuest yeast two-hybrid system with Gateway technology. The NSP4 full-length clone of 528 nt was subjected to specific deletions to construct two 3' deletion mutants, nt 1 to 321 and nt 1 to 450; three 5' deletion mutants, nt 135 to 528, nt 304 to 528, and nt 336 to 528; and two 5' and 3' deletion mutants, nt 240 to 420 and nt 270 to 450.

laser source. The 523/DF35 nm and HQ598/40 filters were utilized to capture FITC and Texas Red fluorescence, respectively, with the transfected cells. Typical settings were as follows: iris = 2.0, laser power = 1 to 3%, gain = 1,000 to 1,250, and black level = -6. The settings used with the virus-infected cells were a 598/40-nm filter, an iris setting of 2.5, a gain of 1,230, and a low-signal boost for Texas Red, while a 530/40-nm filter, an iris setting of 2.2, a gain of 1,230, and a low-signal boost were used for FITC. A 30% power level setting was used in addition to Kalman averaging ($n = 4$) and a $3\times$ digital zoom to refine the subcellular fluorescence signals. To evaluate the extent to which the fluorescence of the FITC and Texas Red panels colocalized in transfected and infected cells, LaserSharp 3.0 (Bio-Rad) and Metamorph version 3.6 software (Universal Imaging Corp., West Chester, PA) were used to construct the images and fluorograms from individual photomultiplier tube signals.

Pixel fluorograms from the Texas Red and FITC components were generated for each set of data to minimize spectral bleedthrough of each signal into the other channel (data not shown). In this way, overlapping pixels belonging to both the Texas Red (red) and FITC (green) channels in the original image could be selected and shown separately (see Fig. 3C, far right). This was accomplished by calculation of the colocalization coefficients for each channel with the equations

$$C_{\text{green}} = \frac{\sum_i I_i^g \delta_{gr}(i)}{\sum_i I_i^g}$$

$$C_{\text{red}} = \frac{\sum_i I_i^r \delta_{rg}(i)}{\sum_i I_i^r}$$

where C_{red} and C_{green} are the colocalization coefficients, I_i^r and I_i^g represent the red and green intensities of the i th pixel after background subtraction, and

$\delta_{rg}(i)$ and $\delta_{gr}(i)$ are Kronecker deltas that represent intensity-independent colocalization weights (36, 39).

Note that for every i th pixel, $\delta_{rg}(i) = \delta_{gr}(i) = 0$ if only a red intensity or a green intensity exists but not both, whereas $\delta_{rg}(i) = \delta_{gr}(i) = 1$ only if both a red and a green intensity are associated with the i th pixel. Hence, a coefficient indicates the fraction of the total intensity that is colocalizing with both fluorescent probes.

Yeast two-hybrid screening. The ProQuest two-hybrid system (Invitrogen) was used to identify potential interactions of NSP4 and caveolin-1. *Saccharomyces cerevisiae* strain MaV203 (*MAT α leu2-3,112 trp1-901 his3 Δ 200 ade2-101 gal4 Δ gal80 Δ SPAL10::URA3 GAL1::lacZ HIS3_{UASGAL1}::HIS3 LYS2 Can1^r Cyh2^r) was used for all two-hybrid analyses (71, 72). A collection of yeast strains that contain plasmid pairs expressing fusion proteins with a spectrum of interaction strengths {pPC97 [GAL4 DNA-binding domain (DBD), *LEU2*], pPC97-CYH2^s, and pPC86 [GAL4 activating domain (AD), *TRP1*] } were used as controls (22, 30, 71, 72). Control plasmids pDBleu and pEXP-AD507 contain only the GAL4 DBD and the GAL4 AD, respectively. A series of yeast transformations were performed to determine the efficiency of the transformation protocol and to test the individual plasmid efficiency of transformation (data not shown).*

NSP4 and caveolin-1 yeast constructs. All plasmid manipulations were performed according to standard protocols with *Escherichia coli* DH5 α as described in the Gateway System manual (2a). Overlapping NSP4 N-terminal (nucleotides [nt] 135 to 528, nt 304 to 528, and nt 336 to 528), C-terminal (nt 1 to 321 and nt 1 to 450), and combined N- and C-terminal (nt 240 to 420 and nt 270 to 450) deletion mutations were PCR amplified from pcDNA3.1-NSP4 with the forward and reverse primers depicted in Fig. 1. Caveolin-1 was amplified from pCCaveolin-1 (a gift from R. Anderson, Southwestern Medical School, Dallas, TX) with forward primer BP12 (5'-ATGTCTGGGGGCAAATA-3') and reverse primer BP13 (5'-ATATCTCGAGTTATATTTCTTCTGCAAGTTGAT-3' [the underlined sequence is a 3' XhoI site]). The PCR products were directionally cloned into Gateway System entry vector pENTR11 (Invitrogen), sequence verified, subcloned into the destination vectors of the Gateway Expression System, pDEST22 ([AD]-X) and pDEST32 ([DBD]-Y), and transformed into MaV203 (2a). Briefly, 300 ng of the pENTR11-NSP4/caveolin-1 plasmids was incubated with 300 ng of the linearized destination vector pDEST22 or pDEST32, LR buffer,

Tris-EDTA (1×), and the LR Clonase enzyme mix (Invitrogen). The resultant clones were transformed into DH5 α and plated onto Luria-Bertani plates with 100- μ g/ml ampicillin or 7- μ g/ml gentamicin. Following amplification, recombinant plasmids were extracted with the Wizard miniprep kit (Promega, Madison, WI); restriction enzyme digested with EcoRV, KpnI, or XhoI (Promega); and sequence verified as pDEST22- and pDEST32-NSP4 or -caveolin-1. Both fusion proteins were individually transformed into *S. cerevisiae* MaV203 to test each clone for self-activation and determine the concentration of 3-amino-1,2,4-triazole (3AT) required to titrate basal HIS3 expression levels.

Yeast two-hybrid assay. To screen for NSP4 and caveolin-1 interactions, two sets of bait (GAL4 DBD) and prey (GAL4 AD) fusion proteins were assayed as DBD-caveolin-1 with AD-NSP4 and as DBD-NSP4 with AD-caveolin-1. Yeast strain MaV203 was transformed by a modified lithium acetate procedure as previously described (22). Transformants were grown at 30°C for 3 days on complete synthetic medium lacking leucine and tryptophan (CSM-Leu⁻ Trp⁻) and replica plated onto the following media to determine the induction of the reporter genes *URA3*, *HIS3*, and *lacZ*: CSM-Leu⁻ Trp⁻ Ura⁻, CSM-Leu⁻ Trp⁻ plus 0.2% 5-fluoroorotic acid (5FOA), and CSM-Leu⁻ Trp⁻ His⁻ plus 3AT (12.5, 50, and 100 mM 3AT).

β -Gal assays. For qualitative measurement of β -galactosidase (β -Gal) expression, transformed yeast was plated onto yeast-peptone-adenine-dextrose medium plates containing a nitrocellulose filter. The presence of β -Gal was detected by the addition of X-Gal (5-bromo-4-chloro-3-indolyl- β -D-galactopyranoside). To quantitatively measure β -Gal activity, chlorophenol red- β -D-galactopyranoside (CPRG) was used as the substrate (2a).

Yeast fusion protein detection. Fusion protein expression levels were monitored by Western blotting. Yeast protein extracts were prepared with the Zymo yeast protein extraction kit (Zymo Research, CA). Briefly, cells were grown in yeast-peptone-adenine-dextrose medium overnight at 30°C and 10⁶ cells were pelleted and resuspended in Y-Lysis buffer with Zymolyase for 1 h at 37°C. The cells were pelleted again and resuspended in PBS, pH 7.2, containing protease inhibitors (100 μ M AEBSF, 80 nM aprotinin, 5 μ M bestatin, 1.5 μ M E-64, 2 μ M leupeptin, 1 μ M pepstatin A, and 100 μ M PMSF), and protein was quantified by bicinchoninic acid assay. Equivalent amounts of protein were loaded onto 12% SDS-PAGE gels for Western blot analysis as described above.

Coimmunoprecipitation and endoglycosidase treatment. MDCK cells were grown as described above and infected with RV SA11 at an MOI of 2 PFU/cell. At 24 hpi, infected and noninfected monolayers were harvested with equal volumes of SDS-free RIPA buffer. Equal volumes of lysates were immunoprecipitated with rat anti-caveolin-1₁₆₁₋₁₇₈ or rat preimmune serum, followed by the addition of protein G-agarose (6% slurry diluted 1:25; Pierce). The agarose beads were pelleted and boiled in sample reducing buffer, and equal volumes were separated by SDS-PAGE and electrotransferred to nitrocellulose membranes. The membranes were blotted with rabbit anti-NSP4₁₅₀₋₁₇₅ and horseradish peroxidase-conjugated goat anti-rabbit IgG. Antibody-specific proteins were visualized by chemiluminescence (described above).

To ensure that the multiple immunoreactive bands were NSP4 specific, uninfected (control) and RV-infected MDCK cell lysates were treated with endo H. Briefly, glycoprotein denaturing was completed in accordance with the manufacturer's (New England Biolabs, Ipswich, MA) directions. Samples were then mock treated or digested with endo H for 1 h at 37°C. The treated lysates were resolved by SDS-PAGE, electrotransferred to nitrocellulose, and probed with NSP4-specific antibody in a Western blot assay. Any shift in NSP4 molecular weight due to glycosidase treatment was visualized by chemiluminescence as described above.

In vitro binding assay. To confirm a direct NSP4-caveolin-1 interaction, synthetic peptides corresponding to NSP4₁₁₃₋₁₄₉, NSP4₁₁₄₋₁₃₅, and NSP4₂₋₂₂ were attached to cyanogen bromide-activated Sepharose 4B beads as recommended by the manufacturer (Amersham Biosciences Corp., Piscataway, NJ). MDCK or FRT cell lysates (100 μ g of protein) were mixed with 50 μ l of a 50% slurry of Sepharose 4B- or Sepharose 4B-NSP4 peptide-bound beads and rotated overnight at 4°C. The beads were pelleted by centrifugation, thoroughly washed, and resuspended in PBS containing protease inhibitors (100 μ M AEBSF, 80 nM aprotinin, 5 μ M bestatin, 1.5 μ M E-64, 2 μ M leupeptin, 1 μ M pepstatin A, 100 μ M PMSF). Equivalent amounts of all samples were separated by 12% SDS-PAGE, electrically transferred to nitrocellulose membranes, and blotted with caveolin-1-specific antibodies (see above, Western blot assay). Negative controls and experiments included FRT cell lysates, NSP4₂₋₂₂-Sepharose-bound beads, and Sepharose beads alone.

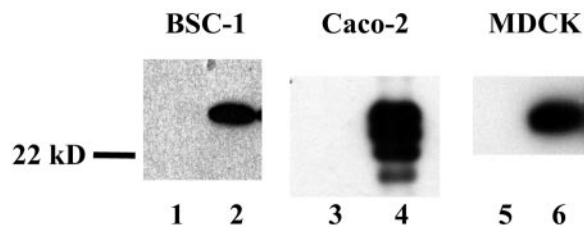


FIG. 2. Transient expression of NSP4 in mammalian cells. BSC-1, Caco-2, and MDCK cells were transiently transfected with pcDNA3.1-NSP4 as described in Materials and Methods. Equal protein concentrations of lysates were separated by 12% SDS-PAGE and electrotransferred to nitrocellulose for Western blot analyses. A specific band for full-length, fully glycosylated NSP4 at ~28 kDa was observed in all three cell lines when probed with rabbit anti-NSP4₁₂₀₋₁₄₇ (lanes 2, 4, and 6). The Caco-2 cells also showed monoglycosylated and unglycosylated, full-length NSP2 (lane 4). Untransfected cell lysates did not show any NSP4-specific bands (lanes 1, 3, and 5).

RESULTS

NSP4 is transiently expressed in mammalian cells. To verify the transient expression of NSP4 in kidney BSC-1 and MDCK cells and intestinal Caco-2 cells, each cell line was transfected with pcDNA3.1-NSP4, grown for 36 h posttransfection, and analyzed by Western blot assay with rabbit anti-NSP4₁₂₀₋₁₄₇. An NSP4-specific band at ~28 kDa was present in all three cell lines, indicating the expression of fully glycosylated, full-length NSP4 (Fig. 2 lanes 2, 4, and 6). The intestinal Caco-2 cells also revealed the mono- and unglycosylated forms of NSP4 (Fig. 2A, lane 4) (see below for endoglycosidase treatment). Untransfected lysates failed to react with the antibody (Fig. 2, lanes 1, 3, and 5).

To evaluate the intracellular location of NSP4 in the absence of other viral proteins, cells were grown in eight-well chamber slides, transfected with pcDNA3.1-NSP4, fixed, and probed sequentially with rabbit anti-NSP4₁₂₀₋₁₄₇ and goat anti-rabbit IgG-FITC. Use of LSCM to monitor the fluorescence signal showed that all of the cell lines (Caco-2, MDCK, and BSC-1) demonstrated comparable levels of NSP4 expression at multiple locations in the cell (Fig. 3A). Reactivity with the NSP4 C-terminal peptide-specific antibody (residues 150 to 175) localized NSP4 to reticular structures surrounding the nucleus, presumably the ER based on previous studies (5, 44, 66, 67), but also to the cytoplasm and at the cell periphery. Primary and secondary antibody controls displayed no background fluorescence (Fig. 3A, left). Although each of the cell lines showed ample NSP4 expression, cytoplasmic vesicle-like structures were most evident in the Caco-2 and MDCK cells (Fig. 3A, cells on the left and in the center), whereas fluorescence near the cell periphery was more pronounced in the MDCK and BSC-1 cell lines (panel A, center and right). The BSC-1 cells (panel A, right) were magnified twofold over the transfected Caco-2 and MDCK cells to facilitate observation of the fluorescent staining distribution. These data clearly demonstrate that NSP4 is present outside of the ER and concur with the punctate staining noted by Berkova et al. (6).

NSP4 and caveolin-1 colocalize. Earlier circular dichroism data suggest that NSP4 and NSP4₁₁₄₋₁₃₅ interact with caveola-like membranes (25, 26). To further explore the possible interaction(s) of NSP4 and caveolae in mammalian cells, colo-

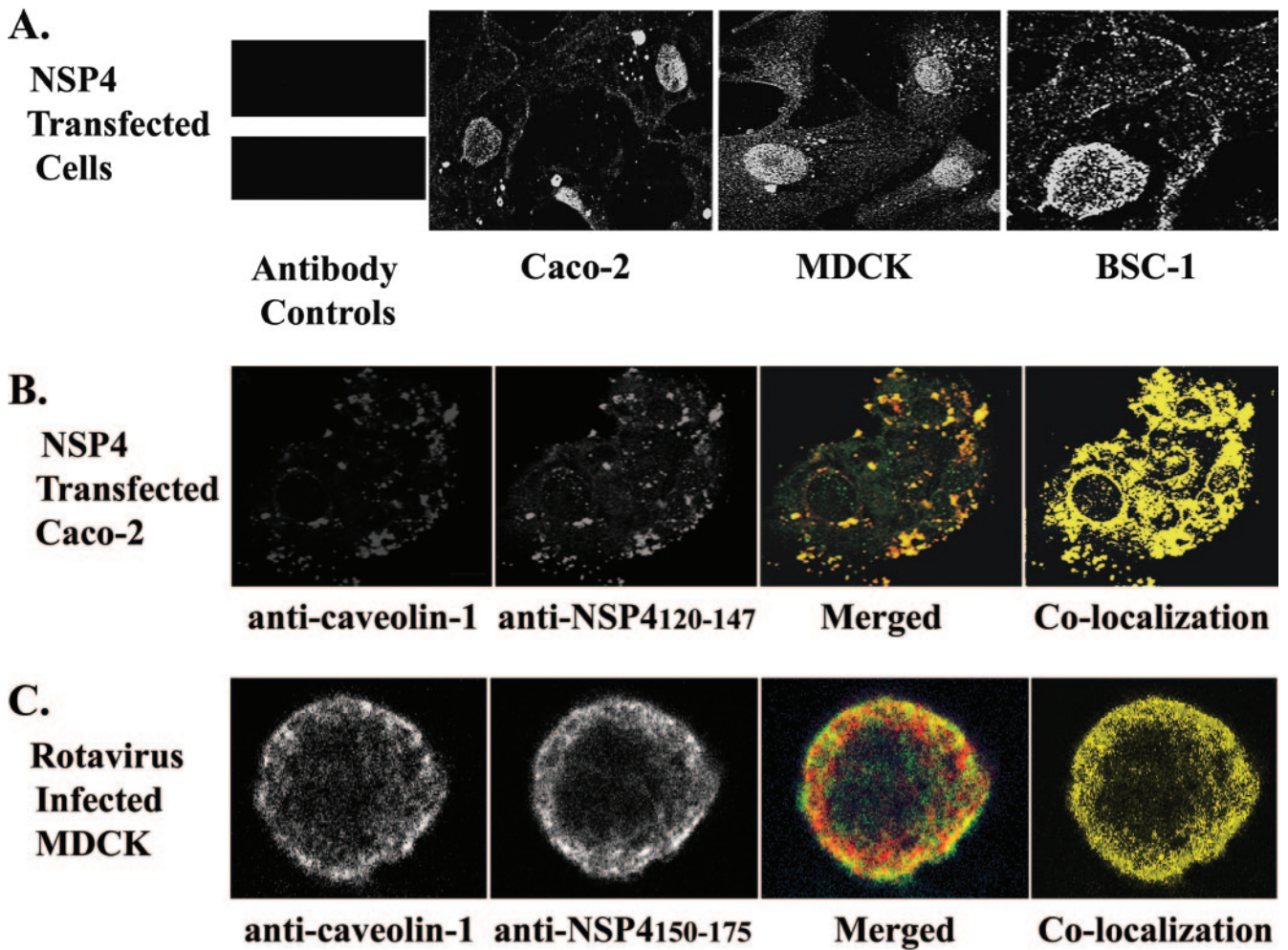


FIG. 3. Confocal imaging and colocalization of NSP4 and caveolin-1. (A) Detection of NSP4 in transiently transfected mammalian cells. Caco-2 (left), MDCK (center), and BSC-1 (right) cultured cells were transfected with pCDNA3.1-NSP4 and probed sequentially with rabbit anti-NSP4₁₂₀₋₁₄₇ and goat anti-rabbit IgG-FITC. The cells were viewed by LSCM with a 63 \times Apochromat oil immersion objective. NSP4 was detected surrounding the nucleus, in vesicular structures in the cytosol, and at the cell periphery. Primary and secondary antibody controls lacked background fluorescence (far left). The BSC-1 cells (far right) are magnified twofold over the Caco-2 and MDCK cells to more easily view the subcellular staining distribution. (B) Colocalization of NSP4 and caveolin-1. Caco-2 cells were transfected with pCDNA3.1-NSP4, grown for 36 h, and fixed with methanol-acetone. Mouse anti-NSP4₁₂₀₋₁₄₇ and rabbit anti-caveolin-1 were used to probe for NSP4 and caveolin-1, respectively, in the same cells. Goat anti-mouse IgG conjugated to FITC and goat anti-rabbit IgG conjugated to Texas Red were used to detect the primary antibodies. Cells were visualized by LSCM with a laser source of 488 and 568 nm. The leftmost panel shows the detection of caveolin-1 (Texas Red) with the Em/Filter = HQ598/40, iris = 2; the next panel shows detection of NSP4 (FITC) with Em/Filter = 523/DF35. The third panel depicts the merged Texas Red and FITC fluorescence images, and the rightmost panel shows the colocalization of caveolin-1 and NSP4 as determined with Universal Imaging Metamorph software, version 3.6. Fluorograms were generated (not shown) and revealed \sim 65% colocalization of NSP4 and caveolin-1. (C) RV-infected MDCK cells were similarly probed and analyzed for caveolin-1 and NSP4 colocalization. As in panel B, caveolin-1 fluorescence is shown on the left, followed by NSP4 and then the merged and colocalized images. For visualization of the infected cells, the settings were a 598/40-nm filter, iris = 2.5, for Texas Red and a 530/40-nm filter, iris = 2.2, for FITC. Fluorograms generated by Metamorph software, version 3.6, disclosed that \sim 73% of the caveolin-1 colocalized with NSP4 in RV-infected cells (data not shown).

calization of NSP4 and caveolin-1, the structural protein of caveolae, was evaluated by LSCM. Before the colocalization study was implemented, it was important to confirm the expression and distribution of caveolin-1 in each cell line. Caco-2, MDCK, and BSC-1 cells were seeded on chamber slides, probed with caveolin-specific antibody, and examined by LSCM. All of the tested cell lines were positive for caveolin-1 in the order of MDCK > Caco-2 \gg BSC-1 based on pixel intensity (data not shown). In addition, the distribution of caveolin-1 at the PM, at the ER, and in the cytoplasm was

similar to that previously reported (2, 48, 55). Because of their intestinal origin, the colocalization results of pCDNA3.1-NSP4-transfected Caco-2 cells are shown (Fig. 3B). Mouse anti-NSP4₁₂₀₋₁₄₇ and goat anti-mouse IgG-FITC again localized NSP4 to perinuclear structures (ER), the cytosol, and the cell periphery (Fig. 3B, center). When the same cells were probed with rabbit anti-caveolin-1 and goat anti-rabbit IgG-Texas Red, caveolin-1 was localized to reticular and vesicular structures, in the cytosol, and at caveolae (panel B, left), as previously shown (2, 48, 55).

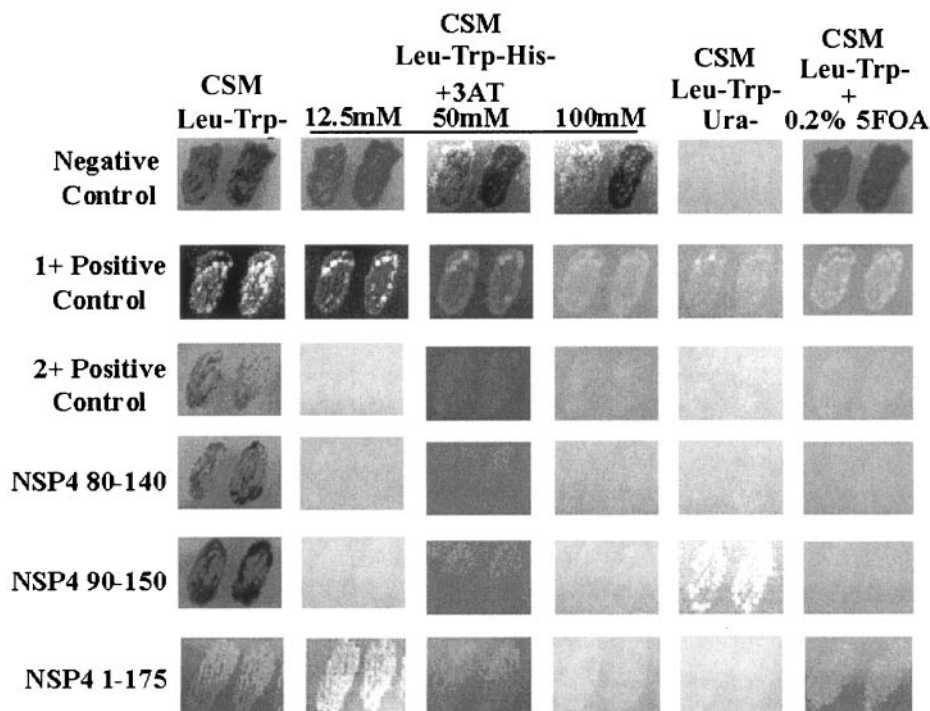


FIG. 4. Representative growth patterns of cotransformed yeast in the reverse yeast two-hybrid assay. MaV203 cells were cotransformed with pDest22caveolin-1 (DBD-caveolin-1) and pDest32NSP4 or pDestNSP432 mutants (AD-NSP4), and growth phenotypes were compared to those of three yeast control strains, negative, weak interaction (1+), and moderate interaction (2+) (top three rows). Individual transformants, pD32NSP4 80-140 (NSP4 nt 240 to 420), pD32NSP4 90-150 (nt 270 to 450), and pD32NSP4 1-175 (nt 1 to 528), were grown on CSM-Leu⁻ Trp⁻ (far left column). Control and test colonies were replica plated onto (i) CSM-Leu⁻ Trp⁻ His⁻ plus 3AT at 12.5, 50, or 100 mM; (ii) CSM-Leu⁻ Trp⁻ Ura⁻; and (iii) CSM-Leu⁻ Trp⁻ plus 0.2% 5FOA. Growth on CSM-Leu⁻ Trp⁻ and CSM-Leu⁻ Trp⁻ His⁻ with ≤ 50 mM 3AT with little to no growth on CSM-Leu⁻ Trp⁻ plus 0.2% 5FOA was considered a weak positive interactor. A moderate positive interaction was indicated by growth on CSM-Leu⁻ Trp⁻ Ura⁻, decreased growth on CSM-Leu⁻ Trp⁻ plus 0.2% FOA (far right panels), and inhibition of growth on CSM-Leu⁻ Trp⁻ His⁻ with ≥ 50 mM 3AT. The stronger the interaction, the greater the growth on the CSM-Leu⁻ Trp⁻ Ura⁻ plates while the growth on CSM-Leu⁻ Trp⁻ plus 0.2% FOA was significantly decreased.

Metamorph program analyses revealed extensive ($\sim 65\%$) colocalization of NSP4 with caveolin-1 (Fig. 3B, right, $n = 5$) in transfected cells. To more readily distinguish colocalizing pixels and the intracellular distribution, fluorograms were generated (not shown), overlapping pixels were selected, and those pixels were visualized (panel B, far right). These data showed extensive colocalization between NSP4 and caveolin-1 in subcellular domains previously shown to contain caveolin-1, i.e., ER, cytosolic vesicles, and caveola microdomains.

To establish that NSP4 colocalizes with caveolin-1 during RV infection, the experiment was repeated with minor variations (see Materials and Methods). A single cell was selected and magnified to enhance visualization of the fluorescent signals. As shown in Fig. 3C (far right), NSP4 colocalized with caveolin-1 in infected MDCK cells. With an MOI of 4 PFU/cell, NSP4 appeared more peripheral in the cell at 20 hpi compared to the transfected cells. Computer analyses showed that $\sim 73\%$ of caveolin-1 and NSP4 colocalized ($n = 13$), somewhat higher than the percentage seen with the transfected cells. Fluorograms were generated to more readily select those pixels that overlapped, i.e., were excited by the FITC and Texas Red probes at equivalent intensities (Fig. 3C, far right). As with the transfected cells, extensive colocalization of NSP4 and caveolin-1 was seen in RV-infected cells. Because peptide-specific antibodies were utilized, the colocalization may in-

clude both the C terminus of the cleavage fragment (77) and full-length NSP4.

NSP4 interacts with caveolin-1 in a yeast two-hybrid assay. LSCM colocalization studies can place proteins within the same organelle of a cell (within 200 nm) but are not sufficient to verify a protein-protein interaction (27). Therefore, the ProQuest Two-Hybrid System was utilized to determine if NSP4 and caveolin-1 directly interact. The sequences encoding NSP4 and caveolin-1 were cloned into yeast two-hybrid vectors pDEST32 and pDEST22 to produce fusion proteins encoding the GAL4 DBD fusion protein (the prey) and AD fusion protein (the bait), respectively. The plasmids were cotransformed into MaV203 and grown on complete synthetic medium plates lacking leucine and tryptophan (CSM-Leu⁻ Trp⁻) with transformation efficiencies of $\sim 2 \times 10^6$ to 5×10^6 transformants/ μg of plasmid DNA, typical of yeast cotransformations (22). To determine the extent to which the active transcription factor for GAL4 was reconstituted by forming dimers between the two fusion proteins, yeast cells were monitored for growth on selective media (Fig. 4). Four phenotypes, His⁺ (3AT^r), β -Gal⁺, Ura⁺, and 5FOA^s, were used to assess the activation of the chromosomally integrated *His3*, *Ura3*, and β -Gal reporter genes. As shown by the representative growth patterns (Fig. 4), all of the transformants and the control yeast

TABLE 1. Phenotypes of pD32-NSP4mutants plus pD22-caveolin-1^a

Peptide	CSM-Leu ⁻ Trp ⁻	CSM-Leu ⁻ Trp ⁻ His ⁻ + 3AT			CSM-Leu ⁻ Trp ⁻ Ura ⁻	CSM-Leu ⁻ Trp ⁻ + 0.2% 5FOA	β-Gal activity (CPRG)	Phenotype ^c
		12.5 mM	50 mM	100 mM				
Negative control	+	+	+	±	-	+	-0.07	Negative
1+ positive control	+	+	+	±	±	±	±0.26	Positive
2+ positive control	+	-	-	-	-	-	+2.44	Positive
NSP4 80-140	+	-	-	-	-	-	+2.20	Positive
NSP4 90-150	+	-	-	-	±	-	+2.17	Positive
NSP4 1-175	+	+	-	-	-	±	±0.29	Positive
NSP4 1-150	+	+	-	-	±	-	+0.42	Positive
NSP4 1-107	+	+	+	±	-	+	-0.06	Negative
NSP4 46-175	+	+	-	-	-	±	+1.39	Positive
NSP4 101-175	+	+	±	-	-	±	+0.36	Positive
NSP4 112-175	+	+	-	-	-	±	+0.70	Positive

^a Colonies were grown on CSM-Leu⁻ Trp⁻ and were replica plated onto CSM-Leu⁻ Trp⁻ His⁻ with 12.5, 50, or 100 mM 3AT; CSM-Leu⁻ Trp⁻ Ura⁻; and CSM-Leu⁻ Trp⁻ with 0.2% 5FOA.

^b β-Gal expression was qualitatively monitored by using X-Gal (not shown), and β-galactosidase activity was quantitatively measured by CPRG assay.

^c The phenotype was determined by combining the results from the differential media.

grew on CSM-Leu⁻ Trp⁻ plates, confirming the presence of pDest32NSP4 and pDest22caveolin-1 or the control plasmids.

Overall growth patterns on selective media were evaluated and compared to known phenotypes (2a). Induction of the *HIS3* gene was shown by dose-dependent growth inhibition on CSM-Leu⁻ Trp⁻ His plus 3AT (12.5 mM, 50 mM, and 100 mM). Decreased growth with increased 3AT was seen, indicative of a positive interaction. A basal level of *HIS3* was produced at the lowest 3AT concentration, 12.5 mM, except for the strong 2+ positive control and NSP4₉₀₋₁₅₀ (Fig. 4). As expected, the negative control yeast cells were not inhibited by any of the concentrations of 3AT and showed growth (Fig. 4). To further demonstrate the interaction of NSP4 and caveolin-1, *URA3* induction was evaluated by (i) growth on plates containing CSM-Leu⁻ Trp⁻ Ura⁻ and (ii) inhibition of growth on plates containing CSM-Leu⁻ Trp⁻ plus 0.2% 5FOA. *URA3* has a weak promoter sometimes producing an intermediate level of *URA3* expression, resulting in both growth on CSM-Leu⁻ Trp⁻ plus 0.2% 5FOA and no growth on plates lacking uracil (2a). Growth patterns for both full-length NSP4 and all seven mutant forms (Fig. 1) with caveolin-1 were evaluated in this manner (Table 1). In addition, induction of *lacZ* was measured qualitatively for the presence of β-Gal (X-Gal) and quantitatively for β-Gal activity (CPRG). Full-length NSP4 and the 1+ positive control produced 0.29 and 0.26 U of β-Gal activity, respectively, whereas the negative control essentially produced no β-Gal activity (Table 1, column 7). As the NSP4 N-terminal hydrophobic domains of NSP4 were removed, there was a progressive increase in β-Gal activity compared to full-length NSP4. This may reflect the different abilities of the fusion proteins to cross the nuclear membrane; i.e., constructs containing one or more of the three NSP4 N-terminal hydrophobic domains may be more readily retained in the membranes of the yeast. This coincides with the β-Gal activity increasing from 0.29 to 2.20 U as additional hydrophobic residues were deleted from the N terminus (Table 1).

Yeast transformed with pD32NSP4 corresponding to aa 1 to 150, aa 80 to 140, aa 90 to 150, aa 46 to 175, aa 101 to 175, and aa 112 to 175 and pD22caveolin-1 demonstrated the positive phenotype His⁺ (3AT^r) Ura^{+/-} 5FOA^s β-Gal⁺ on the selection media (a total of 350 colonies from 12 yeast transforma-

tions), whereas NSP4 aa 1 to 107 produced the negative phenotype Ura⁻ 5FOA^r β-Gal⁻ (Table 1).

To verify that the positive interactions were due to the presence of NSP4 and caveolin-1, GAL-4 fusion proteins were probed with NSP4-specific peptide antibodies or anti-caveolin-1₂₋₃₂ (Fig. 5). Untransformed MaV203 (Fig. 5 lanes 1, 3, 6, 8, and 11) was negative when blotted with all four antibodies. As shown in Fig. 5, all NSP4 (panels A to C) and caveolin-1 (panel D) fusion proteins were expressed and reactive to peptide-specific antisera. The caveolin-1 fusion protein appeared as a dimer in the same cotransformed yeast cell lysates (panel D). Alignment of the positive and negative interactors revealed the binding site of NSP4 to caveolin-1 to be between NSP4 aa 112 and 140.

NSP4 and caveolin-1 coimmunoprecipitate from RV-infected cells. We then evaluated if the NSP4-caveolin-1 interaction occurred in RV-infected mammalian cells. At 24 hpi, RV-infected and uninfected MDCK cells were lysed in SDS-free buffer and immunoprecipitated with rat anti-caveolin-1₁₆₁₋₁₇₈ or preimmune rat antisera. Subsequent Western blot analyses with rabbit anti-NSP4₁₅₀₋₁₇₅ revealed that NSP4-specific bands precipitated from the infected cell lysates with anti-caveolin-1 (Fig. 6A, lane 4). An approximately 30-kDa band was detected in the uninfected lysate control (panel A, lane 2) and was considered a nonspecific background band. The molecular weights of the precipitated bands were the same as those found in RV-infected MDCK cell lysates that had not been reacted with anti-caveolin-1 (panel A, lane 3). There were no NSP4-specific bands detected by Western blot analysis in RV-infected cell lysates precipitated with preimmune serum (panel A, lane 1).

Endo H digestions of the infected and uninfected MDCK cell lysates were evaluated by Western blot analyses. A shift in molecular weight verified that the multiple bands seen in RV-infected cells are NSP4 specific, varying only in glycosylation (Fig. 6B). Precipitation of the doubly glycosylated, singly glycosylated, and unglycosylated forms of NSP4 (28-, 24-, and 20-kDa bands) with caveolin-1 antibody suggests that glycosylation is not critical for the protein-protein interaction (5, 16). The 15- and 18-kDa bands may represent cleavage fragments of NSP4 or multimers of the 7-kDa cleavage product (77).

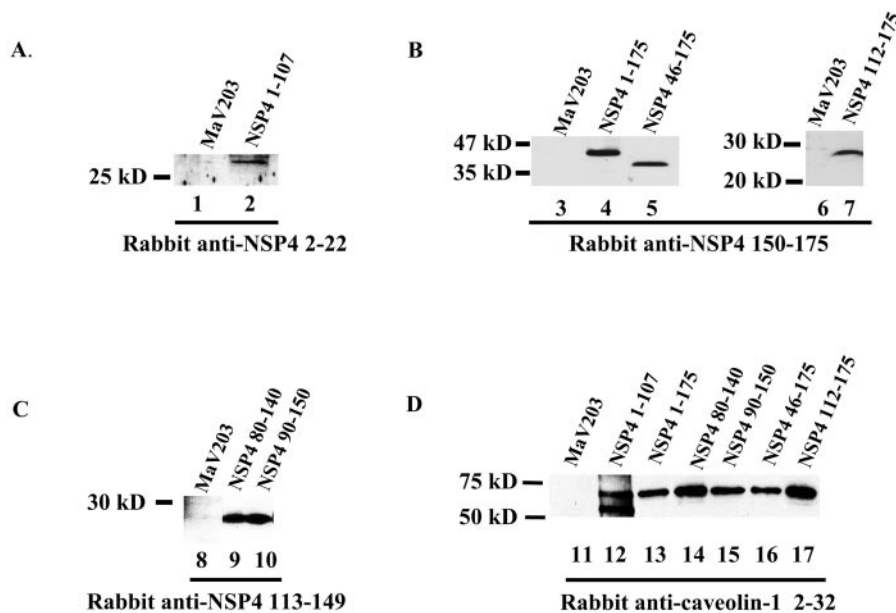


FIG. 5. Western blot analyses of yeast cell lysates cotransformed with full-length NSP4- or NSP4 mutant-caveolin-1 fusion protein. To verify the expression of both the NSP4- and caveolin-1 fusion proteins, the cotransformed MaV203 yeast cell lysates were separated by 12% SDS-PAGE, transferred to nitrocellulose membranes, and probed with rabbit anti-NSP4₂₋₂₂ (lanes 1 and 2), anti-NSP4₁₅₀₋₁₇₅ (lanes 3 to 7), or anti-NSP4₁₁₃₋₁₄₉ (lanes 8 to 10) for NSP4 or NSP4 mutants and anti-caveolin-1₂₋₃₂ (lanes 11 to 17) for caveolin-1. Untransformed controls are shown in lanes 1, 3, 6, 8, and 11.

Although further analyses are needed to distinguish the composition of these bands, these data confirm the interaction of NSP4-caveolin-1 during RV infection of mammalian cells.

NSP4₁₁₃₋₁₄₉ and NSP4₁₁₄₋₁₃₅ peptides capture caveolin-1 from MDCK cell lysates. An *in vitro* binding assay with NSP4-specific synthetic peptides linked to Sepharose beads was developed to confirm the NSP4 caveolin-1 binding domain (aa 112 to 140) determined by yeast-two-hybrid analysis. The Sepharose beads bound to NSP4₁₁₃₋₁₄₉, NSP4₁₁₄₋₁₃₅, or NSP4₂₋₂₂ were incubated with MDCK or FRT cell lysates overnight at 4°C, pelleted, thoroughly washed, separated by 12% SDS-PAGE, and examined by Western blot assay. MDCK cell lysates alone served as the positive control for caveolin-1 antibody reactivity and showed a caveolin-1-specific band at ~22 kDa (Fig. 7, lane 3 in panels A and B; lane 5 in panel C, and lane 4 in panel D). MDCK cell lysates were reacted with beads alone (no bound peptide) to rule out nonspecific binding of caveolin-1 to the Sepharose beads (Fig. 7, lane 1 in panels A and B and lane 2 in panel C). A caveolin-1-specific band at ~22 kDa was detected when MDCK cell lysates were reacted with NSP4₁₁₃₋₁₄₉ (panel A, lane 2). These data agree with the yeast two-hybrid results delineating NSP4 aa 112 to 140 as the binding site for caveolin-1. A positive reaction also was obtained with NSP4₁₁₄₋₁₃₅ (Fig. 7B, lane 2), narrowing the caveolin-1 binding domain to NSP4 aa 114 to 135, the same 21 residues of the enterotoxigenic peptide (4). In contrast, the NSP4₂₋₂₂ peptide failed to capture caveolin-1 from MDCK cells (panel C, lane 3). FRT cell lysates, deficient in caveolin-1 expression, demonstrated no binding to the NSP4 peptide-bound or unbound beads (lanes 1 and 4 in panel C and lanes 2 and 3 in panel D). In agreement with earlier studies (1, 29), FRT cell lysates were negative for caveolin-1 by Western blot assay (panel D, lane 2).

These results complement the data obtained from the *in vivo* yeast two-hybrid assay and further define the NSP4 binding site of caveolin-1 to the enterotoxigenic peptide.

DISCUSSION

The results of this study show an interaction between the RV enterotoxin NSP4 and the caveola structural protein caveolin-1 by yeast two-hybrid analyses, coimmunoprecipitation of infected cell lysates, and an *in vitro* peptide capture assay. Confocal imaging colocalized NSP4 and caveolin-1 at multiple sites in transfected and infected mammalian cells. To our knowledge, this is the first study demonstrating the colocalization and direct interaction of NSP4 and caveolin-1 and the first identification of the caveolin-1 binding domain in the C-terminal region of NSP4. These data corroborate and extend our previous work showing that purified NSP4 and the enterotoxigenic peptide NSP4₁₁₄₋₁₃₅ bind to small unilamellar vesicles (SUVs) with high membrane curvature that are caveola like in composition (25, 26). In that earlier report, we suggest that the NSP4-caveola interaction is lipid mediated as the NSP4 and NSP4₁₁₄₋₁₃₅ helical structures are stabilized by cholesterol and SUVs are exclusively lipid in composition. The preference for negatively charged phospholipids indicates an electrostatic component to the NSP4-lipid vesicle interaction (25, 26). However, a more mobile packing and lower surface pressure of the phospholipids in the outer leaflet compared to the inner leaflet result in an exposed hydrophobic core that may facilitate additional hydrophobic interactions (34, 65). Thus, the interaction is likely more complex than first realized and possibly includes both protein-lipid and protein-protein constituents. It would be in-

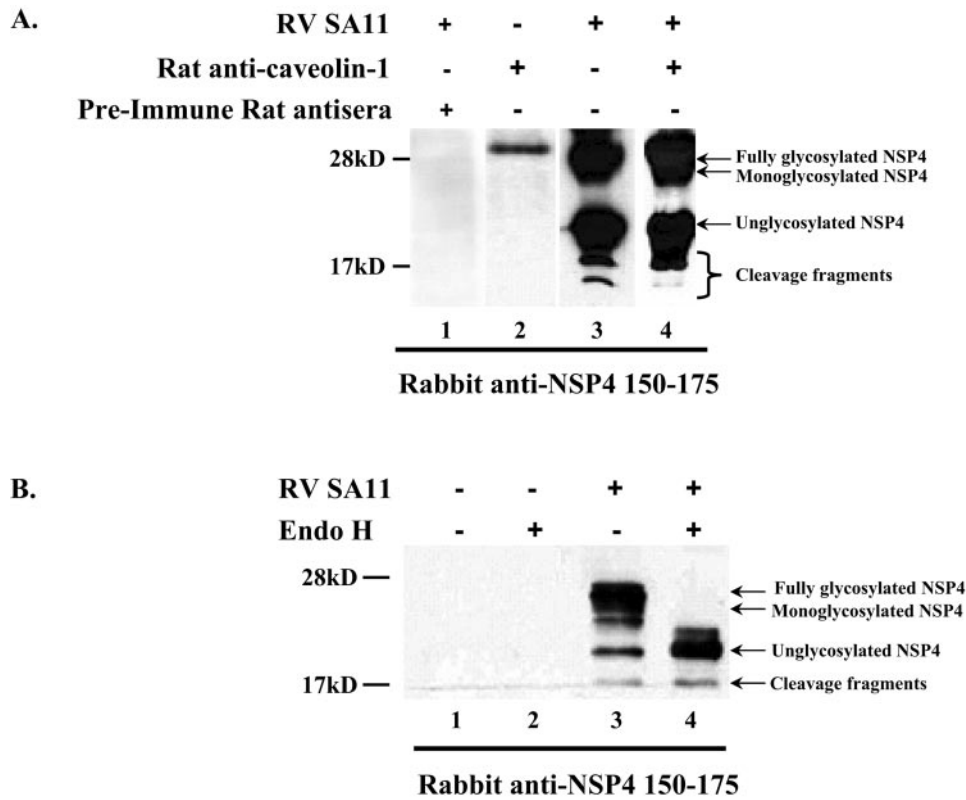


FIG. 6. Coimmunoprecipitation of caveolin-1 and NSP4 from RV-infected MDCK cells. (A) RV-infected (lane 4) and uninfected (lane 2) MDCK cell lysates were reacted with rat anti-caveolin-1₁₆₁₋₁₇₈ and protein G-agarose. The infected MDCK cell lysates were also reacted with rat preimmune sera, which served as a negative control (lane 1). All samples were separated by SDS-PAGE, transferred to nitrocellulose, and blotted with anti-NSP4₁₅₀₋₁₇₅. (A) The absence of NSP4-specific bands from infected MDCK cell lysates precipitated with preimmune serum and uninfected cell lysates reacted with rat anti-caveolin-1₁₆₁₋₁₇₈ are shown in lanes 1 and 2, respectively. Lane 3 contains RV-infected cell lysates alone and serves as the positive control. Full-length, fully glycosylated, monoglycosylated, and unglycosylated NSP4 are present in lanes 3 and 4. Additional bands at ~18 and 15 kDa are reactive with the NSP4 peptide antisera and likely are cleavage products (lanes 3 and 4). A background band at ~30 kDa is present in the uninfected negative control (lane 2). (B) To verify that the ~26- and 24-kDa bands correspond to the monoglycosylated and fully glycosylated forms of NSP4, infected and uninfected MDCK cell lysates were endo H digested, separated by SDS-PAGE, transferred, and blotted with rabbit anti-NSP4₁₅₀₋₁₇₅. Lanes 1 and 3 correspond to the undigested negative and positive controls, respectively. Comparison of lanes 3 and 4 shows the effects of endo H treatment, with the fully glycosylated and monoglycosylated bands shifting to ~20 kDa, equivalent to unglycosylated NSP4.

interesting to determine if the addition of caveolin-1 to cholesterol-rich SUVs would enhance NSP4 binding.

NSP4 and caveolin-1 were colocalized within 200 nm in transiently transfected and RV-infected mammalian cells. Strong staining was observed in the juxtannuclear region and peripheral sites in both transfected and infected cells. Caveolin-1 staining was similar to that observed in previously reported studies, predominantly in cell surface caveolae with additional staining in juxtannuclear reticular structures (ER, Golgi) and in the cytosol associated with either vesicles or soluble complexes (2, 48, 49, 56). Hence, NSP4 peripheral staining that colocalizes with caveolin-1 is potentially within 200 nm of the caveolin-1-containing PM caveolae. Evaluation of the NSP4-caveolin-1 complex immunoprecipitated from RV-infected MDCK cells with anti-caveolin-1 revealed fully glycosylated, monoglycosylated, and unglycosylated forms of NSP4, as confirmed by endo H digestion. In addition, an ~15-kDa cleavage fragment of NSP4 was precipitated that may be a dimer of the reported 7-kDa cleavage fragment (77). These data indicate that NSP4-caveolin-1 binding is independent of

glycosylation. However, glycan chains can induce local changes in protein structure and dynamics, in particular in receptor binding, and thus the role of glycosylation warrants further investigation (35).

A panel of deletion mutant forms of NSP4 was utilized in the yeast two-hybrid assay to map the NSP4-caveolin-1 binding site to NSP4 aa 112 to 140. This is consistent with the physical data reporting an amphipathic alpha-helical coiled-coil region in the extended C-terminal cytoplasmic domain of NSP4 that could serve as a potential binding site for other molecules (8, 44, 68). Using NSP4-specific peptides to capture caveolin-1 from MDCK cell lysates, an *in vitro* binding assay confirmed the aa 112-to-140 binding domain and further delineated the binding site to NSP4 residues 114 to 135, as summarized in Fig. 8. FRT cell lysates lacking caveolin-1 were utilized as a control and failed to bind NSP4 peptides. However, it is possible that NSP4 binds a caveolin-1-associated molecule that is expressed in MDCK cells but not FRT cells.

Previous data show that NSP4 and the enterotoxigenic peptide are less structured when cholesterol is removed from model

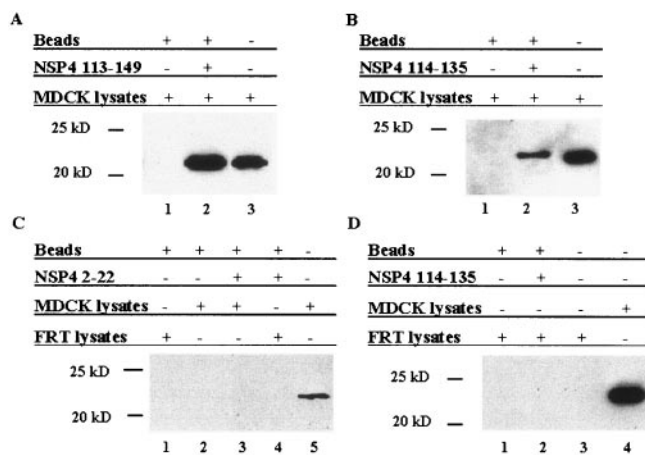


FIG. 7. Refinement of the location of the caveolin-1 binding domain to NSP4 residues 114 to 135. In vitro binding assays were performed with NSP4 peptides 113 to 149 (A), 114 to 135 (B and D), and 2 to 22 (C) attached to cyanogen bromide-activated Sepharose 4B beads. MDCK (A, B, and C) and FRT (C and D) cell lysates were incubated with the immobilized peptide overnight, pelleted, and subjected to Western blot analysis with anti-caveolin-1 antibody. To make sure that the antibody was reactive in the Western blot assays, MDCK cell lysates alone were included in each panel (far right lane of each panel). To ensure the absence of nonspecific binding to the beads, MDCK cell lysates were reacted with peptide-free Sepharose 4B beads (lane 1 in panels A and B and lane 2 in panel C). FRT cell lysates were reacted with beads only (panel C, lane 1) and with both NSP4₂₋₂₂- and NSP4₁₁₄₋₁₃₅-bound beads (lane 4 in panel C and lane 2 in panel D, respectively) and served as an additional negative control. Test lanes for NSP4 peptide-caveolin-1 binding included lane 2 in panels A, B, and D and lanes 3 (MDCK cell lysates) and 4 (FRT cell lysates) in panel C.

membranes and there is a significant loss of peptide binding to cholesterol-depleted SUVs (25, 26). This cholesterol effect on NSP4-lipid interactions mimics that of the caveolin-1 cholesterol dependence in that caveolin-1 structure is altered when cholesterol is removed from cells or from model membranes (61). Caveolin-1 not only binds cholesterol but preferentially incorporates into cholesterol-enriched membranes and functions to transport cholesterol between caveolae and internal organelle membranes (61, 70). One way in which caveolin-1 transports newly synthesized cholesterol from the ER, through the cytosol, to PM caveolae is via a soluble complex composed of hsp56, cyclophilin A, cyclophilin 40, and cholesterol (70). In addition, caveolin-1 has a constitutive, bidirectional transport cycle from caveolae to the ER, through the ER-Golgi intermediate compartment, to the Golgi, and back to the PM (12, 19, 60). These caveolin-1-dependent cholesterol pathways have been shown in MDCK (23), human fibroblast (60, 70), NIH 3T3 (70), and MA104 (61) cells. The critical role of caveolin-1 in cholesterol homeostasis is discussed in detail by Hailstones et al. (23). We now report that NSP4 not only preferentially interacts with cholesterol-rich membranes but also binds caveolin-1. We propose that NSP4 may associate with cholesterol-caveolin-1 complexes and that this interaction may contribute to the transport of NSP4 from the ER to the PM and allow NSP4 to avoid Golgi glycosylases.

Several studies suggest that RV and NSP4 interact with lipid rafts during assembly. Sapin et al. (52) showed that mature

RV, VP4, and NSP4 associate with Triton X-100 detergent-resistant membranes during infection and that VP4 and purified virions interact with model membranes resembling lipid rafts. Those authors suggest that VP4 utilizes rafts as a platform for assembly and NSP4 is necessary for the final stages of RV morphogenesis (52). In a separate study, newly synthesized RV associates with rafts both in vitro and in vivo during the replication process; these data indicate that infectious RV is transported to the cell surface by a raft-dependent pathway (14). An earlier study corroborates RV transport to the PM for release by showing vectorial transport and release of RV from apical membranes that utilizes a nonconventional vesicular pathway that bypasses the Golgi complex (28). Lipid association in viral assembly is not unique to RV in that several enveloped viruses interact with rafts during viral assembly and release. For example, assembly and budding of RSV occur at lipid rafts, where the viral proteins colocalize with caveolin-1 (9). Association of RSV with lipid rafts is likely important in viral pathogenesis by generating filamentous particles and promoting syncytium formation (38). Additional viruses, such as measles virus, vesicular stomatitis virus, human immunodeficiency virus type 1, and Ebola virus, are dependent on raft associations for assembly and budding (10, 13, 37, 42, 73). We agree with the earlier prediction that the association of NSP4 with caveolin-1 or caveolae may contribute to the final steps of RV morphogenesis (52).

Caveolae were first recognized as specialized plasmalemmal microdomains containing a variety of signal transduction molecules (2, 32, 57). These include G protein-coupled receptors, G proteins, small GTPases, adenylyl cyclase, and molecules involved in the regulation of intracellular calcium homeostasis (20, 21, 31, 62, 63). The long list of signal transduction molecules enriched in caveolae suggests that close association of multiple interacting molecules to a single microdomain may actively contribute to cellular responses to specific external stimuli (59). Given the compartmentalization of specific signaling cascades and modulation of the function of resident signaling molecules at caveolae (45, 59), it seems reasonable to speculate that caveolae serve as a site that regulates signal integration, including that of the PI signaling event initiated by extracellular NSP4. In addition, caveolae can be either open or closed at the cell surface, yielding endocytic or exocytic compartments (57, 58). One can envision the possibility of exogenously added NSP4 interacting with signaling molecules localized to rafts or caveolae, but there is no evidence that this occurs.

Localization of the caveolin-1 binding site to enterotoxin residues 114 to 135 adds to the multitude of functions attributed to the NSP4 C-terminal region. The VP6, VP4, and tubulin binding sites map to NSP4 residues 161 to 175, 112 to 148, and 129 to 175, respectively (Fig. 8). NSP4 residues 95 to 137 correspond to the oligomerization domain that folds as an amphipathic coiled coil, and the cleavage site has been localized to aa 112 (5, 8, 68, 77). Despite these advances, many questions remain. For example, what is the NSP4 transport pathway, and how is it regulated? Which of NSP4 residues 114 to 135 are critical to caveolin-1 binding? What are the effects of blocking the NSP4-caveolin-1 interaction on RV replication and disease? Additional studies are required to elucidate the functional connection between NSP4

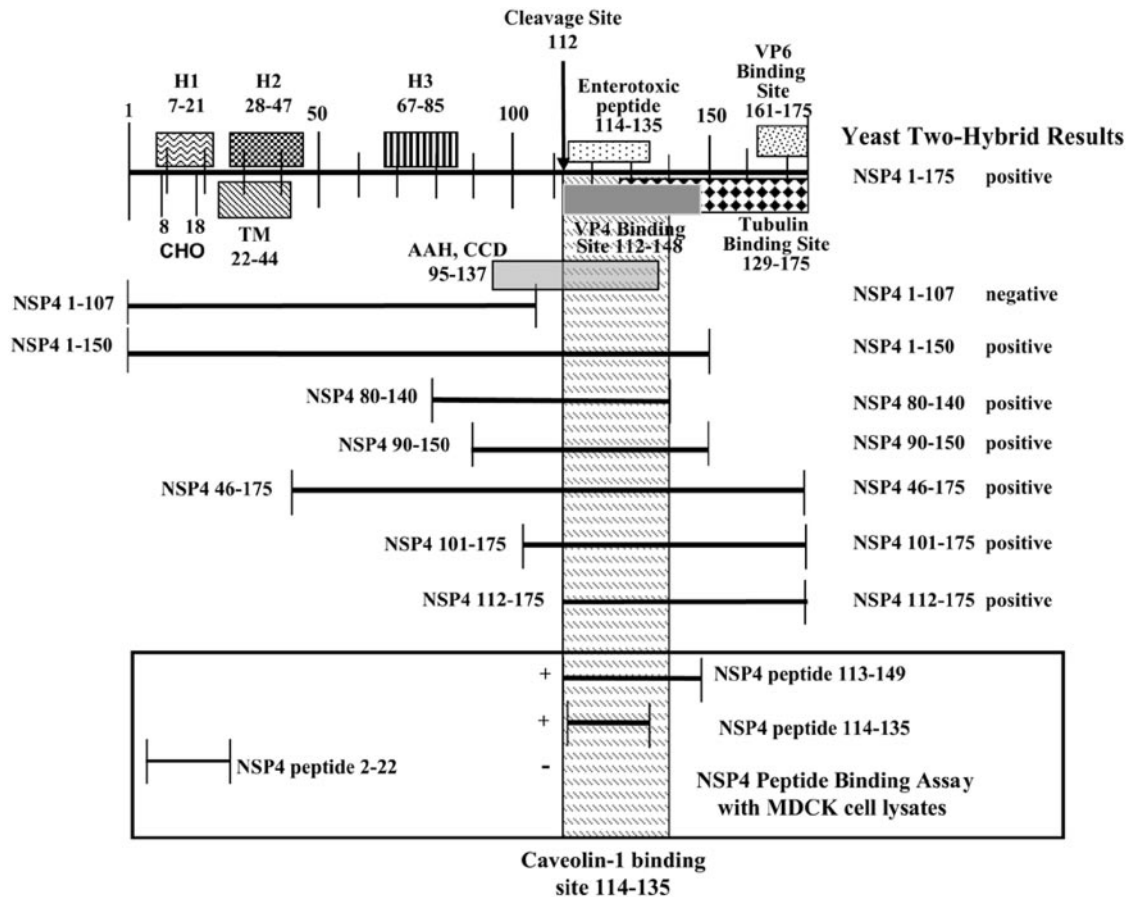


FIG. 8. Alignment of previously reported NSP4 domains with results from the yeast two-hybrid and in vitro capture assays. Selected known functional domains of NSP4 are shown, with H1, H2, and H3 indicating the three N-terminal hydrophobic domains. Glycosylation sites (CHO) are shown at aa 8 and 18. Most of H2 and a small part of H1 traverse the ER membrane such that residues 1 to 23 are localized in the ER lumen and aa 44 to 175 are cytoplasmic. The amphipathic α -helical region that folds as a coiled-coil domain (AAH/CCD, aa 95 to 137), the enterotoxigenic peptide (aa 114 to 135), and the cleavage site at residue 112 are indicated in the extended cytoplasmic domain. The NSP4 binding sites for VP4, VP6, and tubulin are delineated at aa 112 to 148, 161 to 175, and 129 to 175, respectively. The NSP4 deletion mutants are linearly depicted, with the yeast two-hybrid results shown on the right. The alignment of the positive interactions localized the caveolin-1 binding site to NSP4 residues 112 to 140. The results from the peptide capture assays are represented in the lower box, which further defined the caveolin-1 binding site to NSP4 aa 114 to 135.

and caveolin-1 and to determine the role(s) of NSP4-caveolin-1 interaction(s) in NSP4 transport and pathogenesis.

ACKNOWLEDGMENTS

We thank Erin Barth and Pamela Miller for technical assistance.

This research was supported by DHHS/NIH/NIGMS grant GM 62326.

REFERENCES

1. Ambesi-Impombato, F. S., L. A. Parks, and H. G. Coon. 1980. Culture of hormone-dependent functional epithelial cells from rat thyroids. *Proc. Natl. Acad. Sci. USA* **77**:3455-3459.
2. Anderson, R. G. W. 1998. The caveolae membrane system. *Annu. Rev. Biochem.* **67**:199-225.
- 2a. Anonymous. 2002. ProQuest two-hybrid system with Gateway Technology manual. Invitrogen Life Technologies, Carlsbad, Calif.
3. Ball, J. M., D. M. Mitchell, T. F. Gibbons, and R. D. Parr. 2005. Rotavirus NSP4: a multifunctional viral enterotoxin. *Viral Immunol.* **18**:27-40.
4. Ball, J. M., P. Tian, C. Q. Y. Zeng, A. P. Morris, and M. K. Estes. 1996. Age-dependent diarrhea induced by a rotaviral nonstructural glycoprotein. *Science* **272**:101-104.
5. Bergmann, C. C., D. Maass, M. S. Poruchynsky, P. H. Atkinson, and A. R. Bellamy. 1989. Topology of the non-structural rotavirus receptor glycoprotein NS28 in the rough endoplasmic reticulum. *EMBO J.* **8**:1695-1703.
6. Berkova, Z., A. Morris, and M. K. Estes. 2003. Cytoplasmic calcium measurement in rotavirus enterotoxin-enhanced green fluorescent protein (NSP4-EGFP) expressing cells loaded with Fura-2. *Cell Calcium* **34**:55-68.
7. Boshuizen, J. A., J. W. A. Rossen, C. K. Sitaram, F. F. P. Kimenai, Y. Simons-Oosterhuis, C. Laffeber, H. A. Büller, and W. C. Einerhand. 2004. Rotavirus enterotoxin NSP4 binds to the extracellular matrix proteins laminin-B3 and fibronectin. *J. Virol.* **78**:10045-10053.
8. Bowman, G. D., I. M. Nodelman, O. Levy, S. L. Lin, P. Tian, T. J. Zamb, S. A. Udem, B. Venkataraghavan, and C. E. Schutt. 2000. Crystal structure of the oligomerization domain of NSP4 from rotavirus reveals a core metal-binding site. *J. Mol. Biol.* **304**:861-871.
9. Brown, G., J. Aitken, H. W. Rixon, and R. J. Sugrue. 2002. Caveolin-1 is incorporated into mature respiratory syncytial virus particles during virus assembly on the surface of virus-infected cells. *J. Gen. Virol.* **83**:611-621.
10. Brown, E. L., and D. S. Lyles. 2005. Pseudotypes of vesicular stomatitis virus with CD4 formed by clustering of membrane microdomains during budding. *J. Virol.* **79**:7077-7086.
11. Brunet, J.-P., J. Cotte-Laffiette, C. Linxe, A.-M. Quero, M. Geniteau-Legendre, and A. Servin. 2000. Rotavirus infection induces an increase in intracellular calcium. *J. Virol.* **74**:2323-2332.
12. Conrad, P. A., E. J. Smart, Y.-S. Ying, R. G. W. Anderson, and G. S. Bloom. 1995. Caveolin cycles between plasma membrane caveolae and the Golgi complex by microtubule-dependent and microtubule-independent steps. *J. Cell Biol.* **131**:1421-1433.
13. Cook, D. G., J. Fantini, S. L. Spitalnik, and F. Gonzalez-Scarano. 1994.

- Binding of human immunodeficiency virus type 1 (HIV-1) gp120 to galactosylceramide (GalCer): relationship to the V3 loop. *Virology* **201**:206–214.
14. **Cuadras, M. A., and H. B. Greenberg.** 2003. Rotavirus infectious particles use lipid rafts during replication for transport to the cell surface *in vitro* and *in vivo*. *Virology* **313**:308–321.
 15. **Dong, Y., C. Q.-Y. Zeng, J. M. Ball, M. K. Estes, and A. P. Morris.** 1997. The rotavirus enterotoxin NSP4 mobilizes intracellular calcium in human intestinal cells by stimulating phospholipase C-mediated inositol 1,4,5-triphosphate production. *Proc. Natl. Acad. Sci. USA* **94**:3960–3965.
 16. **Ericson, B. L., D. Y. Graham, B. B. Mason, H. H. Hanssen, and M. K. Estes.** 1983. Two types of glycoprotein precursors are produced by the simian rotavirus SA11. *Virology* **127**:320–332.
 17. **Estes, M. K.** 2001. Rotaviruses and their replication, p. 1747–1789. *In* D. M. Knipe, P. M. Howley, and D. E. Griffin (ed.), *Fields virology*. Lippincott-Raven Publishers, Philadelphia, Pa.
 18. **Field, F. J., E. Born, S. Murthy, and S. N. Mathur.** 1998. Caveolin is present in intestinal cells: role in cholesterol trafficking? *J. Lipid Res.* **39**:1938–1950.
 19. **Fielding, C. J., and P. E. Fielding.** 1997. Intracellular cholesterol transport. *J. Lipid Res.* **38**:1503–1521.
 20. **Fujimoto, T.** 1993. Calcium pump of the plasma membrane is localized in caveolae. *J. Cell Biol.* **120**:1147–1157.
 21. **Fujimoto, T., S. Nakade, A. Miyawaki, K. Mikoshiba, and K. Ogawa.** 1992. Localization of inositol 1,4,5-triphosphate receptor-like protein in plasmalemmal caveolae. *J. Cell Biol.* **119**:1507–1513.
 22. **Gietz, R. D., and R. A. Woods.** 2002. Transformation of yeast by lithium acetate/single-stranded carrier DNA/polyethylene glycol method. *Methods Enzymol.* **350**:87–96.
 23. **Hailstones, D., L. S. Sleer, R. G. Partoamd, and K. K. Stanley.** 1998. Regulation of caveolin and caveolae by cholesterol in MDCK cells. *J. Lipid Res.* **39**:369–379.
 24. **Halaihel, N., V. Lievin, J. M. Ball, M. K. Estes, F. Alvarado, and M. Vasseur.** 2000. Direct inhibitory effect of rotavirus NSP4(114–135) peptide on the Na⁺-D-glucose symporter of rabbit intestinal brush border membrane. *J. Virol.* **74**:9464–9470.
 25. **Huang, H., F. Schroeder, M. K. Estes, T. McPherson, and J. M. Ball.** 2004. Interaction(s) of rotavirus non-structural protein 4 (NSP4) C-terminal peptides with model membranes. *Biochem. J.* **380**:723–733.
 26. **Huang, H., F. Schroeder, C. Q. Y. Zeng, M. K. Estes, J. Schoer, and J. M. Ball.** 2001. Membrane interactions of a novel viral enterotoxin: rotavirus nonstructural glycoprotein NSP4. *Biochemistry* **38**:13231–13243.
 27. **Inoue, S.** 1995. Foundations of confocal scanned imaging in light microscopy, p. 1–17. *In* J. B. Pawley (ed.), *Handbook of biological confocal microscopy*. Plenum Press, New York, N.Y.
 28. **Jourdan, N., M. Maurice, D. Delautier, A.-M. Quero, A. Servin, and G. Trugnan.** 1997. Rotavirus is released from the apical surface of cultured human intestinal cells through nonconventional vesicular transport that bypasses the Golgi apparatus. *J. Virol.* **71**:8268–8278.
 29. **Kim, C. H., Y. S. Park, K. N. Chung, and P. C. Elwood.** 2002. Sorting and function of the human folate receptor is independent of the caveolin expression in Fisher rat thyroid epithelial cells. *J. Biochem. Mol. Biol.* **35**:395–402.
 30. **Landy, A.** 1989. Dynamic, structural, and regulatory aspects of lambda site-specific recombination. *Annu. Rev. Biochem.* **58**:913–949.
 31. **Li, S., T. Okamoto, M. Chun, M. Sargiacomo, J. E. Casanova, S. H. N. I. Hansen, and M. P. Lisanti.** 1995. Evidence for a regulated interaction between heterotrimeric G proteins and caveolin. *J. Biol. Chem.* **270**:15693–15701.
 32. **Lisanti, M. P., P. E. Scherer, J. Vidugiriene, Z. Tang, A. Hermanowski-Vosatka, Y. H. Tu, R. F. Cook, and M. Sargiacomo.** 1994. Characterization of caveolin-rich membrane domains isolated from an endothelial-rich source: implications for human disease. *J. Cell Biol.* **126**:111–126.
 33. **Lopez, S., and C. F. Arias.** 2003. Attachment and post-attachment receptors for rotavirus, p. 143–163. *In* U. Desselberger and D. Gray (ed.), *Viral gastroenteritis*. Elsevier Science BV, Amsterdam, The Netherlands.
 34. **Machida, K., and S. I. Ohnishi.** 1980. Effect of bilayer membrane curvature on activity of phosphatidylcholine exchange protein. *Biochim. Biophys. Acta* **596**:201–209.
 35. **Mandal, T. K., and C. Mukhopadhyay.** 2001. Effect of glycosylation on structure and dynamics of MHC class I glycoprotein: a molecular dynamics study. *Biopolymers* **59**:11–23.
 36. **Manders, E. M. M., F. J. Verbeek, and J. A. Aten.** 1993. Measurement of co-localization of objects in dual-color confocal images. *J. Microsc.* **169**:375–382.
 37. **Manie, S. N., S. Debreyne, S. Vincent, and D. Gerlier.** 2000. Measles virus structural components are enriched into lipid raft microdomains: a potential cellular location for virus assembly. *J. Virol.* **74**:305–311.
 38. **McCurdy, L. H., and B. S. Graham.** 2003. Role of plasma membrane lipid microdomains in respiratory syncytial virus filament formation. *J. Virol.* **77**:1747–1756.
 39. **McIntosh, A. L., A. M. Gallegos, B. P. Atshaves, S. M. Storey, D. Kannoju, and F. Schroeder.** 2003. Fluorescence and multiphoton imaging resolve unique structural forms of sterol in membranes of living cells. *J. Biol. Chem.* **278**:6384–6403.
 40. **Meyer, J. C., C. C. Bergmann, and A. R. Bellamy.** 1989. Interaction of rotavirus cores with the nonstructural glycoprotein NS28. *Virology* **171**:98–107.
 41. **Michelangeli, F., F. Liprandi, M. E. Chemello, M. Ciarlet, and M.-C. Ruiz.** 1995. Selective depletion of stored calcium by thapsigargin blocks rotavirus maturation but not the cytopathic effect. *J. Virol.* **69**:3838–3847.
 42. **Nayak, D. P., E. K. Hui, and S. Barman.** 2004. Assembly and budding of influenza virus. *Virus Res.* **106**:147–165.
 43. **Newton, K., J. C. Meyer, A. R. Bellamy, and J. A. Taylor.** 1997. Rotavirus nonstructural glycoprotein NSP4 alters plasma membrane permeability in mammalian cells. *J. Virol.* **71**:9458–9465.
 44. **O'Brien, J. A., J. A. Taylor, and A. R. Bellamy.** 2000. Probing the structure of rotavirus NSP4: a short sequence at the extreme C terminus mediates binding to the inner capsid particle. *J. Virol.* **74**:5388–5394.
 45. **Okamoto, T., A. Schlegel, P. Scherer, and M. P. Lisanti.** 1998. Caveolins, a family of scaffolding proteins for organizing “preassembled signaling complexes” at the plasma membrane. *J. Biol. Chem.* **273**:5419–5422.
 46. **Parashar, U. D., E. G. Hummelman, J. S. Bresee, M. A. Miller, and R. I. Glass.** 2003. Global illness and deaths caused by rotavirus disease in children. *Emerg. Infect. Dis.* **9**:565–572.
 47. **Parr, R. D., and J. M. Ball.** 2003. New donor vector for generation of histidine-tagged fusion proteins using the Gateway Cloning System. *Plasmid* **49**:179–183.
 48. **Parton, R. G.** 1996. Caveolae and caveolins. *Cell Biol.* **8**:542–548.
 49. **Pelkmans, L., J. Kartenbeck, and A. Helenius.** 2001. Caveolar endocytosis of simian virus 40 reveals a new two-step vesicular-transport pathway to the ER. *Nat. Cell Biol.* **3**:473–483.
 50. **Pike, L. J., and L. Casey.** 1996. Localization and turnover of phosphatidylinositol 4,5-bisphosphate in caveolin-enriched membrane domains. *J. Biol. Chem.* **271**:26453–26456.
 51. **Ray, P., J. Malik, R. K. Singh, S. Bhatnagar, R. Bohl, R. Kumar, and M. K. Bhan.** 2003. Rotavirus nonstructural protein NSP4 induces heterotypic antibody responses during natural infection in children. *J. Infect. Dis.* **187**:1786–1793.
 52. **Sapin, C., O. Colard, O. Delmas, C. Tessier, M. Breton, V. Enouf, S. Chwetzoff, J. Ouanch, J. Cohen, C. Wolf, and G. Trugnan.** 2002. Rafts promote assembly and atypical targeting of a nonenveloped virus, rotavirus, in Caco-2 cells. *J. Virol.* **76**:4591–4602.
 53. **Sargiacomo, M., M. Sudol, Z. Tang, and M. P. Lisanti.** 1993. Signal transducing molecules and glycosyl-phosphatidylinositol-linked proteins form a caveolin-rich insoluble complex in MDCK cells. *J. Cell Biol.* **122**:789–807.
 54. **Schnitzer, J. E., P. Oh, B. S. Jacobson, and A. M. Dvorak.** 1995. Caveolae from luminal plasmalemma of rat lung endothelium: microdomains enriched in caveolin, Ca²⁺-ATPase, and inositol trisphosphate receptor. *Proc. Natl. Acad. Sci. USA* **92**:1759–1763.
 55. **Schroeder, F., B. P. Atshaves, A. Gallegos, A. L. McIntosh, J. Liu, A. B. Kier, H. Huang, and J. M. Ball.** 2005. Lipid rafts and caveolae organization, p. 3–36. *In* M. P. Lisanti and P. G. Frank (ed.), *Caveolae and lipid rafts: roles in signal transduction and the pathogenesis of human disease*. Elsevier Academic Press, San Diego, Calif.
 56. **Schroeder, F., A. Frolov, E. J. Murphy, B. P. Atshaves, J. R. Jefferson, L. Pu, W. G. Wood, W. B. Foxworth, and A. B. Kier.** 1996. Recent advances in membrane cholesterol domain dynamics and intracellular cholesterol trafficking. *Proc. Soc. Exp. Biol. Med.* **213**:150–177.
 57. **Shaul, P. W., and R. G. W. Anderson.** 1998. Role of plasmalemmal caveolae in signal transduction. *Am. J. Physiol.* **275**:L843–L851.
 58. **Shaul, P. W., E. J. Smart, L. J. Robinson, Z. German, I. S. Yuhanna, Y.-S. Ying, R. G. W. Anderson, and T. Michel.** 1996. Acylation targets endothelial nitric-oxide synthase to plasmalemmal caveolae. *J. Biol. Chem.* **271**:6518–6522.
 59. **Smart, E. J., G. A. Graf, M. A. McNiven, W. C. Sessa, J. A. Engelman, P. Scherer, T. Okamoto, and M. P. Lisanti.** 1999. Caveolins, liquid-ordered domains, and signal transduction. *Mol. Cell. Biol.* **19**:7289–7304.
 60. **Smart, E. J., Y.-S. Ying, P. A. Conrad, and R. G. W. Anderson.** 1994. Caveolin moves from caveolae to the Golgi apparatus in response to cholesterol oxidation. *J. Cell Biol.* **127**:1185–1197.
 61. **Smart, E. J., Y.-S. Ying, W. C. Donzell, and R. G. W. Anderson.** 1996. A role for caveolin in transport of cholesterol from endoplasmic reticulum to plasma membrane. *J. Biol. Chem.* **271**:29427–29435.
 62. **Song, K. S., S. Li, T. Okamoto, L. A. Quilliam, M. Sargiacomo, and M. P. Lisanti.** 1996. Co-purification and direct interaction of ras with caveolin, an integral membrane protein of caveolae microdomains. *J. Biol. Chem.* **271**:9690–9697.
 63. **Sowa, G., M. Pypaert, and W. C. Sessa.** 2001. Distinction between signaling mechanisms in lipid rafts vs. caveolae. *Proc. Natl. Acad. Sci. USA* **98**:14072–14077.
 64. **Swaggerty, C. L., H. Huang, W. S. Lim, F. Schroeder, and J. M. Ball.** 2004. Comparison of SIVmac239(352–382) and SIVsmmPBj41(360–390) enterotoxic synthetic peptides. *Virology* **320**:243–257.
 65. **Talbot, W. A., L. X. Zheng, and B. R. Lentz.** 1997. Acyl chain unsaturation and vesicle curvature alter outer leaflet packing and promote poly(ethylene glycol)-mediated membrane fusion. *Biochemistry* **36**:5827–5836.

66. Taylor, J. A., and A. R. Bellamy. 2003. Interaction of the rotavirus nonstructural glycoprotein NSP4 with the viral and cellular components, p. 225–235. *In* U. Desselberger and J. Gray (ed.), *Viral gastroenteritis*. Elsevier Science, Amsterdam, The Netherlands.
67. Taylor, J. A., J. C. Meyer, M. A. Legge, J. A. O'Brien, J. E. Street, V. J. Lord, C. C. Bergmann, and A. R. Bellamy. 1992. Transient expression and mutational analysis of the rotavirus intracellular receptor: the C-terminal methionine residue is essential for ligand binding. *J. Virol.* **66**:3566–3572.
68. Taylor, J. A., J. A. O'Brien, and M. Yeager. 1996. The cytoplasmic tail of NSP4, the endoplasmic reticulum-localized nonstructural glycoprotein of rotavirus, contains a distinct virus binding and coiled-coil domains. *EMBO J.* **15**:4469–4476.
69. Tian, P., M. K. Estes, Y. Hu, J. M. Ball, C. Q. Y. Zeng, and W. P. Schilling. 1995. The rotavirus nonstructural glycoprotein NSP4 mobilizes Ca^{2+} from the endoplasmic reticulum. *J. Virol.* **69**:5763–5772.
70. Uittenbogaard, A., Y.-S. Ying, and E. J. Smart. 1998. Characterization of a cytosolic heat-shock protein-caveolin chaperone complex. *J. Biol. Chem.* **273**:6525–6532.
71. Vidal, M. 1997. The reverse two-hybrid system, p. 109. *In* P. A. F. S. Bartel (ed.), *The two-hybrid system*. Oxford University Press, New York, N.Y.
72. Vidal, M., R. K. Brachmann, A. Fattaey, E. Harlow, and J. D. Boeke. 1996. Reverse two-hybrid and one-hybrid systems to detect dissociation of protein-protein and DNA-protein interactions. *Proc. Natl. Acad. Sci. USA* **93**:10315–10320.
73. Vincent, S., D. Gerlier, and S. N. Manie. 2000. Measles virus assembly within membrane rafts. *J. Virol.* **74**:9911–9915.
74. Xu, A., A. R. Bellamy, and J. A. Taylor. 2000. Immobilization of the early secretory pathway by a virus glycoprotein that binds to microtubules. *EMBO J.* **19**:6465–6474.
75. Yuan, L., S.-I. Ishida, S. Honma, J. T. Patton, D. C. Hodgins, A. Z. Kapikian, and H. Hoshino. 2004. Homotypic and heterotypic serum isotype-specific antibody responses to rotavirus nonstructural protein 4 and viral protein (VP) 4, VP6, and VP7 in infants who received selected live oral rotavirus vaccines. *J. Infect. Dis.* **189**:1833–1845.
76. Yuan, L., and L. J. Saif. 2002. Induction of mucosal immune responses and protection against enteric viruses: rotavirus infection of gnotobiotic pigs as a model. *Vet. Immunol. Immunopathol.* **87**:147–160.
77. Zhang, M., C. Q. Y. Zeng, A. Morris, and M. K. Estes. 2000. A functional NSP4 enterotoxin peptide secreted from rotavirus-infected cells. *J. Virol.* **74**:11663–11670.